Soft material actuation by atomization

Han-Joo Lee[1] and Kenneth J. Loh[1,2*]

[1] Material Science and Engineering Program, University of California-San Diego, La Jolla, CA 92093, USA
[2] Department of Structural Engineering, University of California-San Diego, La Jolla, CA 92093-0085, USA

[*] Corresponding author e-mail: kenloh@ucsd.edu

Soft robotics are receiving great attention due to its compliant property and its potential for achieving high degree-of-freedom motions, which are essential for mimicking bioinspired systems. Various methods have been developed to actuate soft materials, ranging from pneumatic actuation to implementing phase transformation. However, techniques that involve fluid pressure require tethered tubes and external compressors, whereas phase transformation generally relies on high temperature changes. In this study, a novel method of actuation that employs ultrasonic-atomization-induced phase transformation of liquid embedded in cavities within soft materials is achieved. In short, atomization is achieved by applying ultrasonic waves on a layer of liquid to create capillary waves at the surface, where small droplets are then ejected from the crests. Small droplets generated by atomization drastically increase the evaporation rate without the need to increase the temperature to boiling. In this study, hollow structures were fabricated with a soft elastomer that were partially filled with ethanol. Ultrasonic waves were propagated through a wall of the structure to atomize the embedded ethanol. Atomizing the embedded ethanol demonstrated as high as ~ 10 times faster actuation rates as compared to evaporating bulk ethanol through heating. The results showed that actuation performance could be controlled by adjusting the voltage and frequency of the signal exciting the transducer. Furthermore, repetitive back-and-forth movement without having to cool the structure was successfully validated.

Keywords: Actuation, atomization, elastomer, phase transformation, soft robotics, ultrasonic.

Introduction

Soft robotics have attracted tremendous interests because of their potential to improve the capabilities of traditional hard robotic systems. The hard and rigid materials used in traditional robotics can perform well only in carefully controlled environments, such as in laboratories or factories. Soft robotics, on the other hand, consist of soft and flexible materials without many rigid components[1]. The compliant property of the soft material allows the structure to deform according to its surroundings[2]. As a result, it is capable of absorbing energy during impact, interacting with humans, manipulating fragile items, and traversing through rough and unpredictable terrains[3,4]. The soft nature of the material also provides higher degrees-of-freedom motions without needing any joints or hinges. This wide range of deformation during actuation is similar to muscle-like movements. In fact, one of the most widely used mechanisms for controlling these soft materials is by using pneumatic actuation, where air is pumped into individual cells to locally inflate the structure and induce motion. However, techniques that involve fluid pressure require tethered tubes and external compressors, which can cause the system to become bulky and heavy.

Another popular method for actuating soft materials is by utilizing phase transformation under various applied stimuli. In general, phase transformation implemented in soft robotics can be categorized into two types. The first is phase transition between two different solid states, which includes shape memory alloys (SMA) or responsive polymeric materials. SMAs change phases at certain temperatures, which allows the material to deform and then return to its original shape upon heating. In fact, these alloys were successfully embedded in soft structures to achieve different types of deformations[5-7]. Compared to SMAs, responsive polymers respond to a much greater variety of stimuli, including temperature, light, pH, and humidity[8-11]. For example, several different types of motions were demonstrated,

such as jumping[12] and gripping[13]. The other phase transformation implemented in soft actuation is vaporization from liquid to gas (*i.e.*, boiling and evaporation). The benefit of boiling is that it can achieve significantly large amounts of strain if the phase-change material is sealed inside the soft structure[14]. Evaporation is another form of liquid to gas transformation but is a slower surface phenomenon. The benefit of evaporation is that it does not require as high temperature as boiling, but the slow phase change process limits its application on inflating soft structures. Instead, previous studies utilized responsive materials that deformed as the water inside or near the structure evaporated[15,16].

Although there are many successful examples of soft actuation through phase transformation, they still suffer from certain issues. Most of the aforementioned examples involve controlling the temperature to actuate the soft structures. In such cases, faster phase transformation can be achieved by applying larger driving force (*i.e.*, higher temperature). However, it is preferred to keep temperature change to a minimum, since it could limit the application in unpredictable environments. In addition, controlling temperature could also become more challenging when the soft robotic system is operated in extreme temperatures. Furthermore, high temperatures may also damage the structure, since most conventional soft materials degrade at lower temperatures as compared to rigid materials.

Rather than increasing the temperature to the liquid's boiling point, ultrasonic atomization increases the evaporation rate even at substantially lower temperatures. When a layer of liquid is excited by ultrasonic waves, small droplets are ejected from the surface of the liquid into the surrounding air. The small size of the droplets in the mist enables much faster evaporation as compared to bulk liquid. The technique was first presented by Wood and Loomis[17], and Lang[18] later determined the relationship between droplet size and wave properties. The benefit of using ultrasonic waves over traditional pneumatic atomization is that droplet size can be easily controlled by adjusting the properties of the wave without affecting the mist density. In general, increasing the frequency of the ultrasonic wave results in smaller droplet sizes.

Atomization is already applied in various fields due to these characteristics, especially when precise control of droplet size is critical. Nebulizers apply ultrasonic waves to atomize liquid medicine into mist[19]. The small droplets of drugs are then inhaled by patients through a connected mask or mouthpiece. Electrostatic coating atomizes the substance that should be coated onto a surface[20]. The small droplets are negatively charged so that they can uniformly coat a positively charged surface. Ultrasonic atomization is also applied in areas where faster evaporation is needed. Small particles can be produced by atomizing solutions of components dissolved in solvents[21]. The solvents in the droplets are then dried to obtain small particles of certain sizes. Increasing the humidity through atomizing water can also be applied for dust control in underground mines[22].

The goal of this study is to introduce a novel method of soft material actuation based on ultrasonic-wave-induced phase transformation of liquid embedded in patterned soft materials[23]. Different types of deformations, namely unidirectional extension and bending, were demonstrated, and the effects of atomization on actuation were also characterized. In short, hollow structures were fabricated from soft elastomers with small amounts of ethanol inside. The embedded ethanol was then atomized by propagating ultrasonic waves into the entire soft structure. Instead of raising the temperature to boiling, the small ethanol droplets enabled rapid vaporization into its gas phase. The phase change increased the pressure inside the structure and resulted in actuation. Two different types of deformations were demonstrated by purposefully designing and patterning the structures. An accordion-like structure was fabricated to demonstrate unidirectional deformation. Bending deformation was validated by implementing pneumatic networks (PneuNets) into the soft structure[24]. Then, reversible back-and-forth bending was validated by combining and bonding together two identical bending structures facing in opposite directions to one another. This paper starts with an introduction of ultrasonic atomization. Then, the fabrication method of the structures is discussed, followed by the experimental setup for actuation and characterization. Last, the effects of evaporation and atomization were measured separately to show how much atomization enhances actuation performance as compared to simply heating and evaporating bulk ethanol.

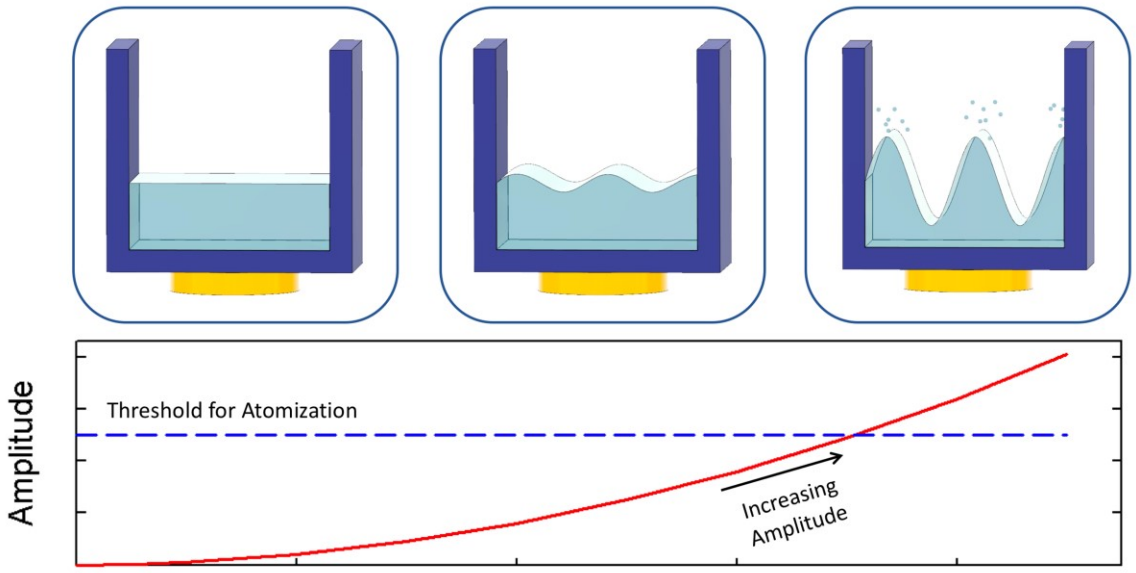

Figure 1. The illustration shows the process of ultrasonic atomization, where a layer of liquid is placed above an ultrasonic transducer. The surface of the liquid stays stationary when the transducer is off (*i.e.*, amplitude is zero). When ultrasonic waves are propagated, capillary waves form on the liquid surface. As the amplitude of the ultrasonic wave increases, a critical point is reached when small droplets are ejected from the crests of the capillary waves.

Atomization background

Ultrasonic atomization is a method that can generate small droplets by propagating ultrasonic waves into a layer of liquid[17]. There are two different hypotheses that explain how these small droplets are generated. The cavitation hypothesis states that cavities are formed in the liquid when an ultrasonic wave is applied[25]. When these cavities collapse near the liquid surface, small droplets are ejected. The capillary wave hypothesis explains that the droplets are formed when the capillary wave on the surface of the liquid becomes unstable[18]. Various studies were conducted to test both hypotheses, and several studies concluded that both cavitation and capillary waves contribute to atomization[26-28]. Nevertheless, the capillary wave hypothesis established a strong correlation between the mean droplet size and excitation frequency, which is still widely used in the field of atomization.

Fig. 1 illustrates how capillary waves result in the ejection of small droplets. Initially, a layer of liquid is placed above an ultrasonic transducer. When the transducer is turned off and does not generate any waves, the surface of the liquid remains stationary. If the transducer is turned on, the surface of the transducer vibrates, creating ultrasonic waves that propagate perpendicular to the surface. As a result, capillary waves are formed at the liquid-air interface. The amplitude of the capillary waves changes in tandem with the amplitude of the ultrasonic wave. However, a critical point is reached when the capillary wave is no longer stable due to its high amplitude. The surface at the crests start to collapse, which results in small droplets being ejected into the air. Since atomization is related to the stability of the liquid surface, surface tension and density of the liquid also contribute important roles.

As mentioned earlier, the size of the droplets can be controlled with uniform size by adjusting the applied ultrasonic wave. Lang[18] described the relationship between the frequency of the applied ultrasonic wave and the size of the droplets. First, the wavelength of the capillary wave can be calculated from:

$$\lambda^3 = \frac{2\pi T}{\rho f^2} \tag{1}$$

where λ is the wavelength of the capillary wave, T is surface tension, ρ is density of the liquid, and f is surface wave frequency. Here, f is half of the excitation wave frequency, F[29]. Since the droplets are generated from the crests of the capillary wave, median droplet diameter, D, is a function of λ. The droplet size can be calculated using:

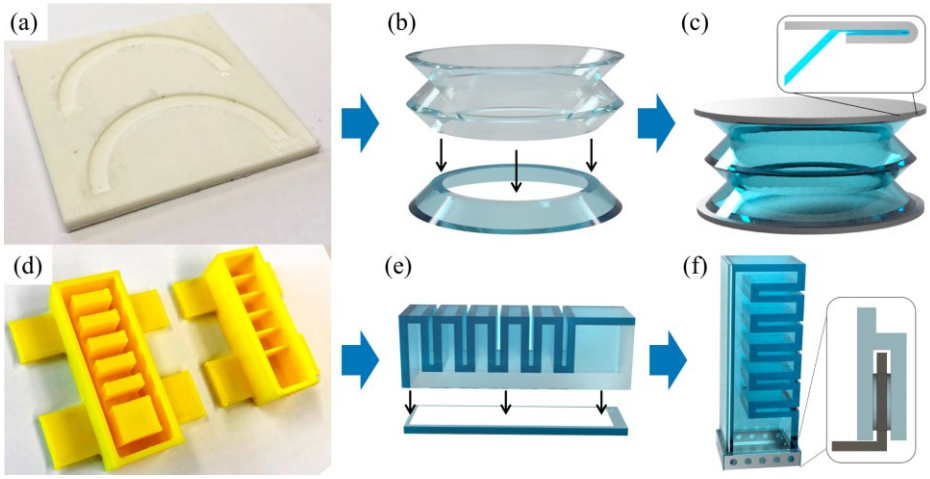

Figure 2. (a) A picture of a 3D printed mold for the unidirectional structure is shown. (b) Bonding the two ends of the strip resulted in a truncated cone structure that can be stacked on top of one another. (c) The edge of the aluminum sheet was folded onto the elastomer to ensure a tight seal. (d) A two-piece mold was 3D printed for fabricating the bendable structure. (e) A piece of paper was embedded in the bottom layer of the elastomer before sealing the bottom side of the structure. (f) The illustration shows the aluminum sheet that was bonded with the elastomer for complete sealing.

$$D = 0.34\left(\frac{8\pi T}{\rho F^2}\right)^{\frac{1}{3}} \tag{2}$$

There are two effects that need to be considered during actuation through atomization. The first is the rapid evaporation rate of the small droplets as compared to its bulk form. Since the method involves expanding the structure through liquid to gas phase change, faster evaporation will result in faster actuation rates. The second effect is the evaporation of the bulk liquid throughout the process. When ultrasonic waves propagate through the structure, ultrasonic heating naturally increases temperature. In this study, the effects of atomization and evaporation will be measured separately to evaluate how atomization improves actuation performance of soft structures.

Experimental Details

Fabrication

Two different soft structures were fabricated to achieve different types of deformations. The first structure was designed to have an accordion-like shape that expands unidirectionally. The second structure was fabricated to have PneuNets of channels to realize bending motion[24]. Both structures were fabricated from FX-Pro elastomer (Smooth-On Inc.), since it is capable of sustaining large deformations and is suitable for soft robotics. The silicone rubber was prepared by hand-mixing two parts (Part A and Part B) with a 1:1 weight ratio. The mixture was then placed in a vacuum chamber before being cured in room temperature.

First, the fabrication procedure of the unidirectional structure is illustrated in Figs. 2(a) to 2(c) and was introduced in a previous study.[23] Fig. 2(a) shows a 3D-printed mold for fabricating elastomer strips. The molds were printed using Ninjaflex, which is a flexible filament, to facilitate removal of the strips. The silicone mixture was then poured into the mold to form a semi-circular strip and was degassed before curing began. After curing, the two ends of the strip were bonded together with the same uncured mixture of FX-Pro to form a truncated cone-shaped structure. As shown in Fig. 2(b), this process was repeated until four of the same structures were stacked on top of one another. More uncured FX-Pro was applied to form a strong bond between the truncated cone shaped structures. Fig. 2(c) is an illustration of the final structure, where thin aluminum sheets were used to seal the top and bottom openings. Thin metal sheets were selected, because they are lightweight and allow the ultrasonic wave to propagate through with little attenuation. Forming a strong bond between the elastomer and the aluminum sheet was crucial too, and this was achieved by folding the edge of the aluminum sheets so that the metal layer held the elastomer in place.

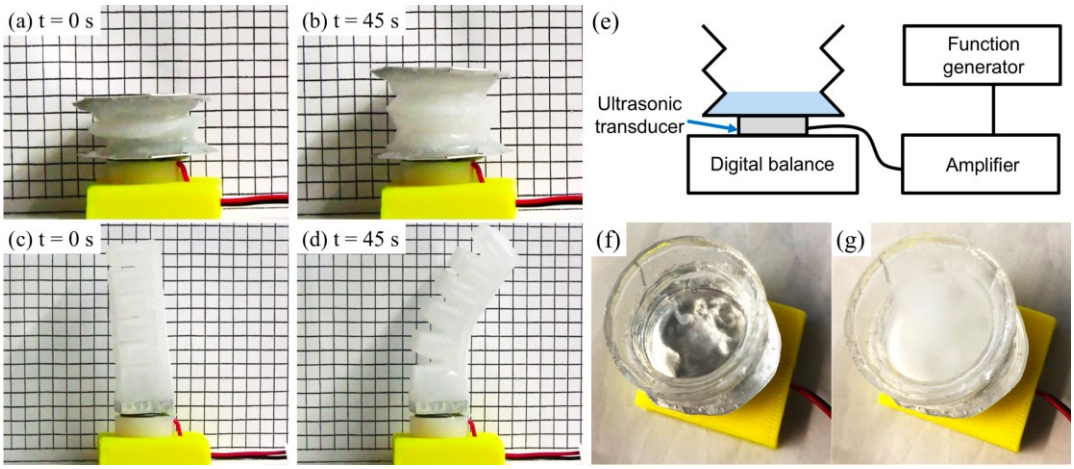

Figure 3. (a) The accordion-like soft structure was placed above the ultrasonic transducer, and, in the background, the grid separation distance is 5 mm. (b) A square wave of 320 V_{pp} and 2.72 MHz was applied to the structure for 45 s, which increased the displacement by ~ 10 mm. (c) A similar setup is shown for the bending structure. (d) The same testing condition resulted in a horizontal displacement of ~ 20 mm. (e) The experimental setup to measure atomization rate is illustrated, where an open-ended structure filled with ethanol was placed above the ultrasonic transducer. The ultrasonic transducer and the structure was placed on a digital balance to measure the weight loss of ethanol during atomization. (f) Applying ultrasonic waves to the open-ended structure resulted in atomization of ethanol. (g) Small droplets are ejected into the air, and, after ~ 30 s, the structure was filled with ethanol mist.

Second, Figs. 2(d) to 2(f) illustrate the fabrication process of the PneuNets bending structure. Fig. 2(d) shows a 3D-printed two-piece mold made of polylactic acid (PLA). After pouring the uncured silicone rubber into the bottom mold, it was degassed slowly before carefully placing the top mold. The cured elastomer is shown in the top part of Fig. 2(e), where the bottom and right side of the structure is still open. A layer of FX-Pro was used to seal the bottom side of the structure, where a sheet of paper was embedded to constrain elongation but still enable bending. This allowed the structure to bend more effectively without having to increase the thickness of the bottom layer. Then, uncured FX-Pro was carefully applied around the layer to bond it with the structure from the mold. Fig. 2(f) shows the sealing of the final structure. The edges of the aluminum sheet were folded 90° with equally spaced holes on the sides. Uncured FX-Pro was applied over the aluminum so that the elastomer held onto the structure through the holes. Furthermore, two additional bending structures were fabricated and bonded together with more uncured FX-Pro to demonstrate rapid and reversible bending movements.

It should be mentioned that, before completely sealing the two structures with aluminum sheets, the samples were partially filled with ethanol. Ethanol was selected since it has a high vapor pressure and a low boiling temperature of 78 °C. The amount of ethanol in the accordion and PneuNet structures was ~ 2.5 mL and ~ 1 mL, respectively, so that the height of the ethanol layer were ~ 4 mm for both structures.

Atomization actuation characterization

Ultrasonic waves were applied to the test structures to validate actuation through atomization of the embedded ethanol. Fig. 3(a) shows the unidirectional sample placed on an ultrasonic transducer that was secured in place by a 3D-printed PLA stage. When voltage is applied to the transducer, mechanical strain is generated. High strain piezoelectric transducers with great electrical to mechanical efficiencies[30] (*i.e.*, greater than 90%) are generally used for atomization. Since the overall efficiency of the system is highly affected by the capability of the transducer to generate waves, the ratio of sound energy output to electrical energy input was estimated[31]. The electrical to sound efficiency of the system was ~ 0.16% when the ultrasonic wave propagated through ethanol. A coupling agent was applied between the sample and the transducer to minimize attenuation at the interface. The overall setup was placed immediately in front of a grid with lines separated by 5 mm. Then, a Keysight 33600A function generator connected to a Ciprian US-TXP-3 voltage amplifier outputting a controlled square-wave signal to actuate the structure. The voltage and frequency were varied to study how these parameters affected actuation performance. In one set of tests, frequency varied from 2.66 MHz to 2.78 MHz in 0.02 MHz increments, while the peak-to-peak voltage (V_{pp}) was fixed at 320 V_{pp}. An actuated

unidirectional structure is shown in Fig. 3(b). In the other set of tests, voltage was adjusted from 320 V_{pp} to 240 V_{pp} in 20 V_{pp} intervals at a fixed frequency of 2.72 MHz. Videos were recorded throughout the tests to evaluate actuation, where the amount of displacement was quantified through image processing of individual video frames. The same experiments were also conducted using the bending structure, where the images before and after turning on the ultrasonic transducer are shown in Figs. 3(c) and 3(d).

To provide an idea of the operating pressure, blocking-stress was measured by conducting similar tests on the unidirectional structure. The blocking-stress was calculated by measuring the load applied by the structure. A load cell was fixed in place directly above the structure before actuation so that the load was measured at a constant displacement (*i.e.*, the soft structures were constrained at their initial undeformed positions). Frequency dependence was measured under a constant voltage of 320 V and the same frequency range of 2.66 MHz to 2.78 MHz. In addition, blocking-stress was also measured when voltage was varied (*i.e.*, from 240 V to 320 V), while frequency was fixed at 2.72 MHz.

Atomization versus evaporation

The next set of experiments were conducted to evaluate how much atomization and evaporation separately contributed to soft structure actuation. Fig. 3(e) illustrates the test setup for measuring the weight loss of ethanol due to atomization. An open-ended structure partially filled with ethanol was placed on top of the ultrasonic transducer. The actuation conditions for atomization was the same as the conditions mentioned previously. The transducer was set above a digital balance to periodically measure the weight loss of ethanol during atomization. In addition, temperature changes of ethanol were recorded using a noncontact infrared thermometer (Fluke, 568 Infrared Thermometer). During this test, the weight of ethanol was recorded for 10 s when the increase in temperature was less than 3 °C. It was assumed that the measured weight loss was only due to atomization without evaporation. Continued atomization would then further increase temperature, and evaporation of ethanol would also start to influence weight loss. However, atomization rate was considered constant even after 10 s, since temperature does not significantly affect surface tension or density of ethanol according to equation (2).

The evaporation rate of ethanol was also measured to study how it affected actuation. First, temperature time histories measured from the aforementioned tests corresponding to different voltage and frequency combinations were used to guide the control of a digital hot plate. The open-ended structure with ethanol was placed on top of the hot plate, while the specimen was heated accordingly and then periodically measuring weight. The decrease in weight of ethanol indicated the amount of liquid that evaporated, which would also contribute to expanding the soft structures if they were sealed. These tests were repeated using the sealed samples to measure how much the structures expanded due to evaporation.

Results and discussion

Soft structure actuation

The goal of implementing atomization for soft material actuation is to promote liquid-to-gas phase change without significantly increasing the temperature of the embedded liquid. As mentioned earlier, ethanol was filled in two types of different soft structures, namely, one designed for unidirectional extension and the other for bending (Fig. 3). All of the tests were conducted for 45 s to attain the deformed states as shown in Figs. 3(b) and 3(d), thereby validating actuation by ultrasonic-wave-induced atomization of ethanol. Figs. 3(f) and 3(g) show the same test conducted on a unidirectional soft structure with one end kept opened. It can be observed from Fig. 3(f) that the propagating ultrasonic waves induced atomization and violent motions of the liquid at the surface. Fig. 3(g) shows that continued atomization ejected mist that filled the structure after ~ 30 s. The small droplets or ejected mist then evaporated. Since evaporation is a surface phenomenon, small droplets evaporate faster than its bulk form due to its high surface-to-volume ratio. The size of the droplets can be calculated from equation (2) and by using an ethanol density of 789 kg/m^3, surface tension of 22.1 mN/m, and the corresponding excitation frequency (*i.e.*, 2.66 MHz to 2.78 MHz). The calculated median droplet diameter is in the sub-micrometer range, which is small enough to consider that the droplets evaporated immediately after being ejected into the air when vapor pressure was still low[32]. It should be mentioned that the tests

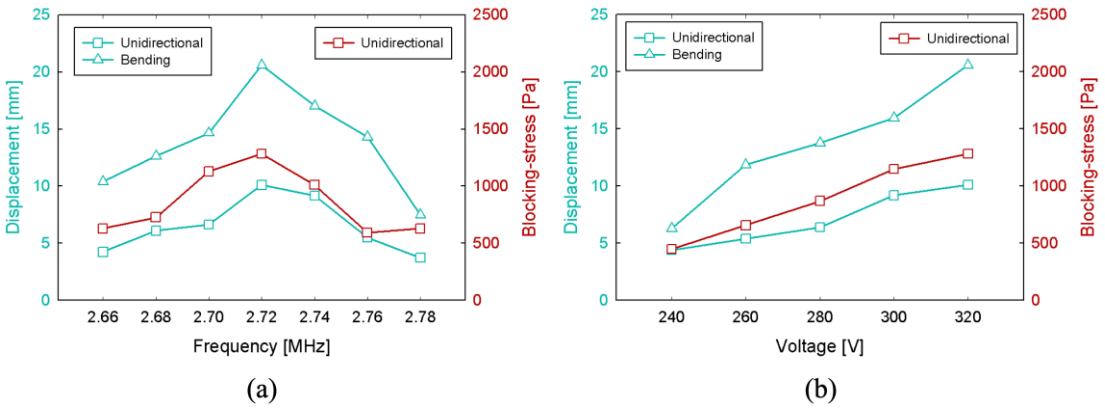

Figure 4. (a) Displacements of the unidirectional and bending samples are plotted against frequency between 2.66 MHz and 2.78 MHz. A constant voltage of 320 V_{pp} was applied, while displacements after 45 s were measured and plotted. Vertical displacement was measured for the unidirectional structure, whereas horizontal displacement was measured for the bending structure. Blocking-stress was also calculated at a constant displacement under the same frequency range. (b) Similar tests were conducted with the input frequency fixed at 2.72 MHz, while the input voltage ranged from 240 V_{pp} to 320 V_{pp}.

were stopped at 45 s and well before the equilibrium vapor pressure of ethanol was reached so as to prevent over-deforming and damaging the samples.

Both the unidirectional and bending soft structures were actuated using the ultrasonic transducer, where the frequencies and input voltages were varied. Vertical displacement was measured for the unidirectional structure, whereas the horizontal displacement of the free-end was measured for the bending structure. Blocking-stress was also calculated for the unidirectional structure, while its displacement was fixed at its initial undeformed position. Figs. 4(a) and 4(b) plot the maximum displacements of the free-end for both types of samples when frequency or voltage was changed, respectively, while keeping the other parameter fixed. Among the frequencies, 2.72 MHz demonstrated the highest deformation rate after 45 s. The unidirectional structure deformed by ~ 10 mm, and the horizontal displacement of the bending structure was ~ 20 mm after actuation. Both structures exhibited lower displacements as the frequency deviated from 2.72 MHz. Fig. 4(b) shows similar tests that were conducted by decreasing the voltage from 320 V_{pp} to 240 V_{pp} at 20 V_{pp} intervals and at a fixed frequency of 2.72 MHz. Decreasing the voltage resulted in lower displacements. Blocking-stress of the unidirectional structure measured under the same testing conditions are also plotted in Figs. 4(a) and 4(b). Similar to the displacement results, the maximum blocking-stress reached ~ 1300 Pa when the transducer was actuated with 2.72 MHz and 320 V_{pp} signals. Increasing or decreasing the frequency resulted in lower stress, as well as decreasing the voltage. It should be noted that the generated blocking-stress followed the same trends for unidirectional actuation and bending, as well as for the different frequencies and voltages tested.

Effects of ultrasonic atomization

It was also explained that the voltage and frequency of the excitation signals were varied for characterizing actuation performance. The atomization rates for the various testing conditions are summarized in Fig. 5. Atomization rate was computed by measuring the amount of weight loss of ethanol over a testing period of ~ 10 s. The assumption was that, in the initial 10 s of testing, the temperature change of ethanol was negligible, so mass loss was due solely to atomization.

In particular, Fig. 5(a) shows the atomization rates when input frequency ranged from 2.66 MHz to 2.78 MHz at a constant voltage of 320 V_{pp}. It is well known that ultrasonic transducers resonate at a certain frequency, which generates the highest amplitude. The amplitude generally decreases as the excitation frequency deviates from its resonant frequency. A similar trend is shown in Fig. 5(a), where 2.72 MHz exhibited the highest atomization rate. Frequencies beyond the plotted conditions did not generate enough amplitude to atomize ethanol. On the other hand, Fig. 5(b) shows the atomization rates when the input voltage was adjusted from 240 V_{pp} to 320 V_{pp}, while frequency was fixed at 2.72 MHz (*i.e.*, as was determined from the previous tests). It is known that increasing the amplitude of the voltage input also increases ultrasonic wave amplitude; this same trend for atomization can be observed in Fig.

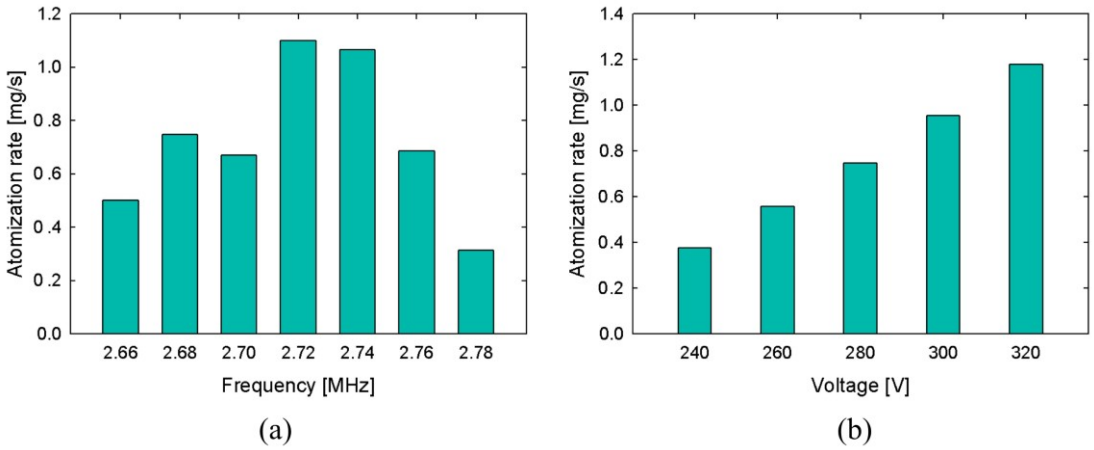

Figure 5. (a) Atomization rate was measured, while the ultrasonic transducer was excited with a voltage of 320 V_{pp} and frequency ranged from 2.66 MHz to 2.78 MHz. (b) Input voltage was controlled from 240 V_{pp} to 320 V_{pp} to study the effects on atomization rate, while frequency was fixed at 2.72 MHz.

5(b). Overall, the change in atomization rate indicates how adjusting input voltage and frequency affected the maximum displacements obtained (*i.e.*, after the same amount of time), as well as the actuation rate or speed of the soft structure.

Effects of temperature-induced evaporation

Since atomization does not boil ethanol, only evaporation contributes to atomization-induced phase change. Thus, to study the contributions of temperature-induced evaporation, open-ended soft structures partially filled with ethanol were prepared. Ultrasonic waves were applied to the structure with the aforementioned conditions, while temperature was measured and plotted in Figs. 6(a) and 6(b). Similar to the atomization rates shown in Fig. 5, 2.72 MHz and 320 V_{pp} demonstrated the highest temperature change. A digital hot plate was employed to heat the sample in a manner similar to how the sample heated up during ultrasonic atomization. Figs. 6(c) and 6(d) summarize the weight loss of ethanol due to temperature-induced evaporation corresponding to different frequency and voltage conditions. The decrease in weight of the sample was strictly due to ethanol that evaporated from liquid to gas and then escaping to the ambient atmosphere due to the use of open-ended test samples. First, for samples where voltage was fixed at 320 V_{pp}, Fig. 6(c) shows that all frequency conditions showed a similar weight loss until ~ 20 s; major differences became clearly visible after 45 s of testing. In general, conditions that induced higher atomization rates (Fig. 5a) resulted in higher temperature changes, thus causing greater weight loss of ethanol as shown in Fig. 6(c). Second, the weight loss of ethanol due to temperature changes corresponding to tests conducted with different excitation voltages is plotted in Fig. 6(d). Overall, the results are similar to Fig. 6(c), where the difference in weight loss became more apparent after ~ 20 s. In addition, higher applied voltages resulted in higher weight loss, which was expected.

Atomization versus evaporation

The total weight loss of ethanol after 45 s was studied and compared to weight loss due to atomization and temperature-induced evaporation. The atomization rate was assumed to be constant throughout the actuation period of 45 s. The total weight loss of ethanol due to both atomization and evaporation for various conditions were considered and plotted in Fig. 7. Fig. 7(a) shows the weight loss of ethanol, while the input frequency varied from 2.66 MHz to 2.78 MHz and at a constant voltage of 320 V_{pp}. The total weight loss reached a maximum value of 66 mg at 2.72 MHz and decreased to a minimum value of 20 mg at 2.78 MHz. Fig. 7(b) plots weight loss with respect to voltage varied from 240 V_{pp} to 320 V_{pp} but at a fixed frequency of 2.72 MHz. The maximum value of 66 mg at 320 V_{pp} decreased with decreasing voltage and reached a minimum of 25 mg at 240 V_{pp}. In general, weight loss due to atomization was much greater than the weight loss due to temperature-induced evaporation.

When the soft structures were excited by the ultrasonic transducer, the total weight loss and displacement are due to the combined effects of atomization and evaporation. In order to compare the relative change in total weight loss and

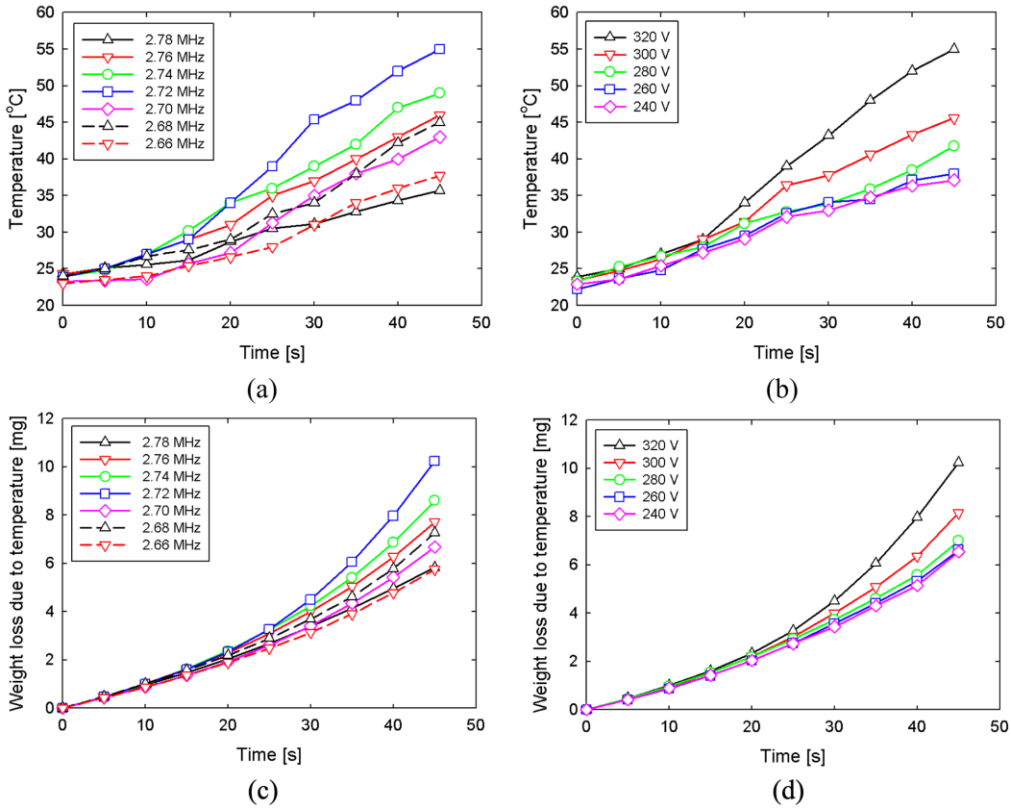

Figure 6. (a) Temperature change was measured and plotted, while the unidirectional structure was actuated with a constant input voltage of 320 V_{pp} and input frequency from 2.66 MHz to 2.78 MHz. (b) Temperature change was plotted, while the structure was actuated with input voltage from 240 Vpp to 320 Vpp and constant frequency of 2.72 MHz. The evaporation of ethanol was measured by employing a hot plate to heat the same structure in a similar manner. (c) The weight loss of ethanol was determined and plotted over the 45 s duration of testing. Results for different frequencies of excitation ranging from 2.66 MHz to 2.78 MHz kept at constant voltage of 320 V_{pp} are shown. (d) A similar set of tests was conducted, except that voltage was varied between 240 V_{pp} and 320 V_{pp} with frequency kept constant at 2.72 MHz.

displacement over different conditions, both results were normalized with respect to their maximum values. The normalized values (N_{norm}) were calculated using:

$$N_{norm} = \frac{N}{N_{max}} \tag{3}$$

where N_{max} is the maximum value, and N is the measured value when tested with different conditions. The normalization was applied to total weight loss, temperature-induced weight loss, and displacement. From Fig. 7(a), it was found that the maximum total weight loss of ethanol was 66 mg when frequency was 2.72 MHz. Thus, the total and temperature-induced weight loss values for each frequency condition was divided by 66 mg to obtain their corresponding relative weight loss of ethanol. Fig. 8(a) compares the relative weight loss and displacement over a range of frequencies at a fixed voltage of 320 V_{pp}. It can be seen that atomization-induced weight loss was as high as ~ 4.5 times greater than weight loss due to evaporation at 2.72 MHz. This ratio generally decreased as the frequency deviated from 2.72 MHz.

A similar normalization was performed on the displacement results of the unidirectional and bending structures shown in Fig. 4. During actuation by the ultrasonic transducer, unidirectional and bending structures reached a maximum displacement of ~ 10 mm and ~ 20 mm, respectively. Thus, the displacement due to the ultrasonic transducer and direct heating for each frequency condition was divided by these maximum values to compare their relative change. In case of actuation by the ultrasonic transducer, the relative decrease in ethanol weight loss and displacements of the two structures followed a similar trend. This indicated that total weight loss, which was mostly due to atomization,

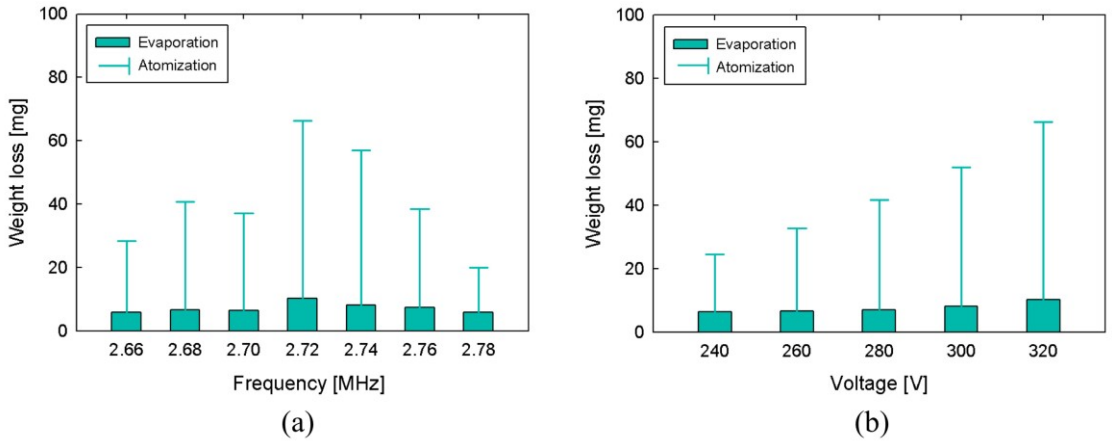

Figure 7. The total weight loss of ethanol after 45 s of testing was characterized based on the effects of both atomization and evaporation. The weight loss due to evaporation was first plotted, followed by adding weight loss due to atomization. (a) The weight loss of ethanol is plotted for different frequency cases while maintaining an input voltage of 320 V_{pp}. (b) Similar tests were conducted to measure weight loss, while input voltage ranged from 240 V_{pp} to 320 V_{pp} with a constant frequency of 2.72 MHz.

plays an important role in actuating the structure. The displacements of both structures deformed by temperature-induced evaporation (*i.e.*, by the hot plate) were significantly lower, which were both ~ 10% of the displacements induced by atomization. As the frequency deviated from 2.72 MHz, the displacements due to evaporation were almost negligible.

The results for relative weight loss and displacements as the excitation voltage was varied is shown in Fig. 8(b). Again, the maximum weight loss and displacement values were used to normalize the results shown in Fig. 4(b) and Fig. 7(b) to generate Fig. 8(b). The general decreasing trends of relative weight loss and displacement were similar as the voltage decreased. Similar to Fig. 8(a), decreasing the voltage reduced the contribution of atomization to total weight loss. In case of results from the ultrasonic transducer, decreasing the voltage to 240 V_{pp} reduced the displacement to ~ 40% for both structures. Displacements of the structures placed on the hot plate also decreased with decreasing voltage and were almost negligible at 240 V_{pp}.

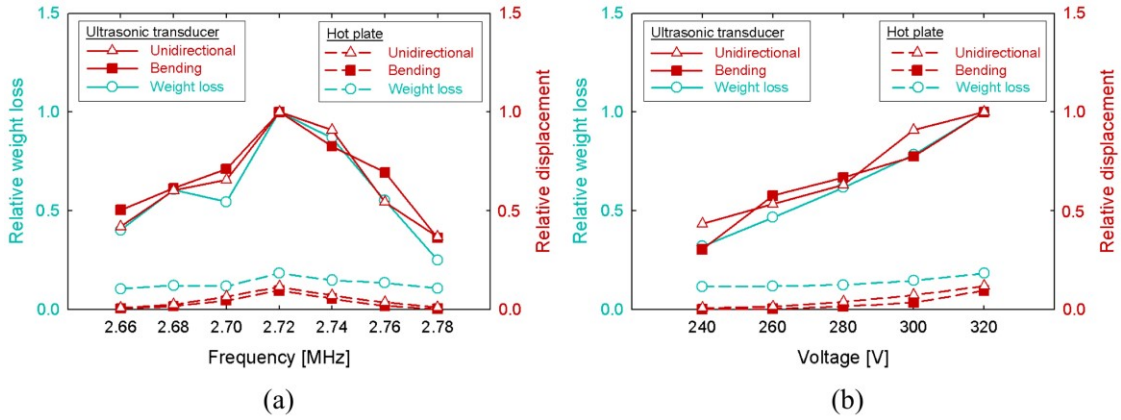

Figure 8. Relative or normalized weight loss was compared with relative displacement for different testing conditions. The results from the ultrasonic transducer indicate weight loss and displacement due to both atomization and evaporation. The effect of evaporation alone was measured by heating the structure with a hot plate. The temperature of the hot plate was controlled following the temperature time histories in Figs. 6(a) and 6(b). (a) Relative weight loss and relative displacement are plotted versus the frequency of excitation. (b) Relative weight loss and relative displacement are plotted as a function of input voltage. All the results indicated that temperature-induced evaporation only contributed a small fraction of the total actuated response of the soft structure.

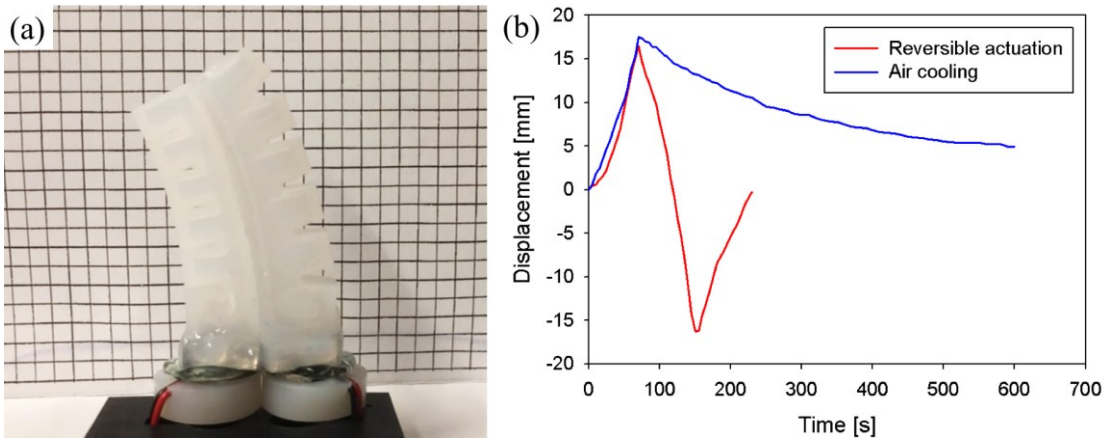

Figure 9. (a) Two bending structures were bonded together for validating reversible actuation. The image shows bending of the structure after actuating the right-hand-side ultrasonic transducer for 70 s. (b) The transducers were sequentially turned on to achieve back-and-forth movement for one full cycle. The horizontal displacement time history result is compared with the displacement of the same structure that was actuated to ~ 16 mm and then allowed to cool.

Reversible actuation

For the final test, the design of the bending structure was modified to validate rapid and reversible actuation. Two bending structures facing opposite directions were bonded together and actuated individually. The transducers were excited using a constant input voltage of 320 V_{pp} at 2.72 MHz. Fig. 9(a) shows an image of the bonded structure after the first ultrasonic transducer was excited for 70 s. Thereafter, the first transducer was turned off, while the second ultrasonic transducer was turned on. Switching of the excitation source allowed the soft structure to bend in the other direction. This procedure was repeated until the soft structure was actuated to move ~ ±16 mm (in both directions) before returning to its initial position (*i.e.*, to displace the free-end by one full cycle). The displacement response of the system is plotted in Fig. 9(b). The results clearly validated that the bending structure could be controlled to deform in either directions and in a fairly repeatable manner.

In addition, a separate test that actuated the same structure to ~ 16 mm was also performed. In this case, upon reaching peak free-end displacement, the actuator was shut off to allow the system to cool and return to its initial position (*i.e.*, to complete one half-cycle of motion). These results are also overlaid in Fig. 9(b). For one half-cycle of motion, it can be seen that sequentially controlling the ultrasonic transducers enabled the system to deform at a significantly faster rate (*i.e.*, >6 times as fast) than relying on cooling (*i.e.*, ~ 115 s versus >600 s). It should be emphasized that, even after 600 s, the displacement of the cooled soft structure was still greater than 5 mm. It should be noted that ethanol condensation from gas to liquid is affected by temperature change, as well as increases in pressure. Actuating the second transducer bends the structure towards the first, which increases the pressure of the inflated channel. The increase in pressure, which is also observed in Fig. 4, contributes to the condensation rate and enhances reversible deformation.

Conclusions

The objective of this paper was to introduce a novel method of soft material actuation, where two different structures partially filled with ethanol were shown to actuate and change their shape when subjected to propagating ultrasonic waves. Unidirectional deformation was achieved using an accordion-like structure, whereas bending was enabled by designing and patterning the soft structure to have PneuNets. First, it was found that ultrasonic-induced atomization of the embedded ethanol ejected small droplets that enhanced the evaporation rate at temperatures well below boiling. The fast evaporation of the small droplets expanded the structure, which was enough to demonstrate different types of deformation. Their deformation could also be controlled by adjusting input voltage and frequency used to excite the ultrasonic transducer. Second, the contributions of atomization- versus temperature-induced actuation to total

deformation was assessed using open-ended soft structures. By measuring the weight loss of ethanol over time and due to atomization and heating separately, it was found that the displacements of both structures due to atomization were ~ 10 times greater than displacements induced by evaporation. Furthermore, reversible actuation was also validated by selectively propagating ultrasonic waves to different portions of a soft material system to induce bending in specific directions. Overall, this study presented a new modality for controlling actuation of soft materials using propagating ultrasonic waves as opposed to directly heating the embedded liquid. Since the method does not require external pumps or tethered tubes, it is expected to be applied to various applications, including locomotion, gripping, and haptic systems. Although promising, these results are still preliminary; before they can be implemented to control soft robotic systems, future work will consider mechanisms for improving actuation speed (or rate).

Acknowledgements

This research was supported by U.S. National Science Foundation under grant no. CMMI-1762530. Additional support was provided by the Jacobs School of Engineering, University of California-San Diego. The authors also thank Prof. Francesco Lanza di Scalea (UC San Diego) for allowing the authors to use their voltage amplifier and other equipment.

References

1. Trivedi, D., Rahn, C. D., Kier, W. M. & Walker, I. D. Soft robotics: Biological inspiration, state of the art, and future research. *Applied Bionics and Biomechanics* **5**, 99-117, (2008).
2. Case, J. C., White, E. L. & Kramer, R. K. Soft Material Characterization for Robotic Applications. *Soft Robotics* **2**, 80-87, (2015).
3. Shepherd, R. F. *et al.* Multigait soft robot. *P Natl Acad Sci USA* **108**, 20400-20403, (2011).
4. Tolley, M. T. *et al.* A Resilient, Untethered Soft Robot. *Soft Robotics* **1**, 213-223, (2014).
5. Lee, Y. P., Kim, B. K., Lee, M. G. & Park, J. O. Locomotive mechanism design and fabrication of biomimetic micro robot using shape memory alloy. *2004 Ieee International Conference on Robotics and Automation, Vols 1- 5, Proceedings*, 5007-5012, (2004).
6. Laschi, C. *et al.* Soft Robot Arm Inspired by the Octopus. *Adv Robotics* **26**, 709-727, (2012).
7. Seok, S. *et al.* Meshworm: A Peristaltic Soft Robot With Antagonistic Nickel Titanium Coil Actuators. *Ieee-Asme Transactions on Mechatronics* **18**, 1485-1497, (2013).
8. Meng, H. & Li, G. Q. A review of stimuli-responsive shape memory polymer composites. *Polymer* **54**, 2199-2221, (2013).
9. Hines, L., Petersen, K., Lum, G. & Sitti, M. Soft Actuators for Small-Scale Robotics. *Advanced Materials* **29**, (2017).
10. Li, M. H. & Keller, P. Artificial muscles based on liquid crystal elastomers. *Philos T R Soc A* **364**, 2763-2777, (2006).
11. Zhou, J. & Sheiko, S. Reversible shape-shifting in polymeric materials. *Journal of Polymer Science Part B-Polymer Physics* **54**, 1365-1380, (2016).
12. Lee, H., Xia, C. G. & Fang, N. X. First jump of microgel; actuation speed enhancement by elastic instability. *Soft Matter* **6**, 4342-4345, (2010).
13. Taccola, S. *et al.* Toward a New Generation of Electrically Controllable Hygromorphic Soft Actuators. *Advanced Materials* **27**, 1668-+, (2015).
14. Miriyev, A., Stack, K. & Lipson, H. Soft material for soft actuators. *Nat Commun* **8**, (2017).
15. Wang, J. R. *et al.* Tunable, Fast, Robust Hydrogel Actuators Based on Evaporation-Programmed Heterogeneous Structures. *Chem Mater* **29**, 9793-9801, (2017).
16. Chen, X. *et al.* Scaling up nanoscale water-driven energy conversion into evaporation-driven engines and generators. *Nat Commun* **6**, (2015).
17. Wood, R. W. & Loomis, A. L. The physical and biological effects of high-frequency sound-waves of great intensity. *Philos Mag* **4**, 417-436, (1927).
18. Lang, R. J. Ultrasonic Atomization of Liquids. *J Acoust Soc Am* **34**, 6-&, (1962).
19. Stevens, H. R. & Albregt, H. B. Assessment of Ultrasonic Nebulization. *Anesthesiology* **27**, 648-&, (1966).
20. Inculet, I. I. & Klein, R. G. Electrostatic painting of nonconductive surfaces with water-base paints. *Ieee T Ind Appl* **32**, 90-92, (1996).
21. Nandiyanto, A. B. D. & Okuyama, K. Progress in developing spray-drying methods for the production of controlled morphology particles: From the nanometer to submicrometer size ranges. *Adv Powder Technol* **22**, 1-19, (2011).
22. Okawa, H., Nishi, K., Kawamura, Y., Kato, T. & Sugawara, K. Utilization of ultrasonic atomization for dust control in underground mining. *Jpn J Appl Phys* **56**, (2017).
23. Lee, H.-J., Funderburk, M. & Loh, K. J. Actuation of soft materials through ultrasonic atomization. *Proc. SPIE* **10593**, (2018).
24. Ilievski, F., Mazzeo, A. D., Shepherd, R. E., Chen, X. & Whitesides, G. M. Soft Robotics for Chemists. *Angew Chem Int Edit* **50**, 1890-1895, (2011).
25. Sollner, K. The mechanism of the formation of fogs by ultrasonic waves. *T Faraday Soc* **32**, 1532-1536, (1936).
26. Yasuda, K., Honma, H., Xu, Z., Asakura, Y. & Koda, S. Ultrasonic Atomization Amount for Different Frequencies. *Jpn J Appl Phys* **50**, (2011).
27. Ramisetty, K. A., Pandit, A. B. & Gogate, P. R. Investigations into ultrasound induced atomization. *Ultrason Sonochem* **20**, 254-264, (2013).
28. Barreras, F., Amaveda, H. & Lozano, A. Transient high-frequency ultrasonic water atomization. *Exp Fluids* **33**, 405-413, (2002).
29. Mahravan, E., Naderan, H. & Damangir, E. Frequency and wavelength prediction of ultrasonic induced liquid surface waves. *Ultrasonics* **72**, 184-190, (2016).

30. Huber, J. E., Fleck, N. A. & Ashby, M. F. The selection of mechanical actuators based on performance indices. *P Roy Soc a-Math Phy* **453**, 2185-2205, (1997).
31. Landau, L. D. & Lifshitz, E. M. *Fluid Mechanics*. Vol. 6 (Butterworth-Heinemann, 1987).
32. Babin, V. & Holyst, R. Evaporation of a sub-micrometer droplet. *J Phys Chem B* **109**, 11367-11372, (2005).